Chinese Chemical Letters 35 (2024) 109148

Contents lists available at ScienceDirect

Chinese Chemical Letters

journal homepage: www.elsevier.com/locate/cclet

A new Keggin-type polyoxometallate-based bifunctional catalyst for trace detection and pH-universal photodegradation of phenol

Shuang Li, Jiayu Sun, Guocheng Liu*, Shuo Zhang, Zhong Zhang*, Xiuli Wang*

College of Chemistry and Materials Engineering, Professional Technology Innovation Center of Liaoning Province for Conversion Materials of Solar Cell, Bohai University, Jinzhou 121013, China

ARTICLE INFO

Article history:
Received 17 August 2023
Revised 8 September 2023
Accepted 25 September 2023
Available online 21 November 2023

Keywords:
POM-based metal-organic complex
Bifunctional catalyst
Phenolic colorimetric sensor
Low detection limit
pH-universal photocatalysis
Photodegraded phenol

ABSTRACT

The widespread application of phenolic substances in the field of food, medicine and industry, is harmful to the environment and human health. Therefore, it is very important to develop a convenient and effective method to detect and degrade phenolic compounds. Herein, we report a new keggin-type polyoxometallate-based metal-organic complex self-assembled under solvothermal condition, $\{[Cu(dap)(3\text{-}PA)]_4(SiW_{12}O_{40})(H_2O)_2\}\cdot 2H_2O$ (**1**, dap = 1,2-diaminopropane, 3-HPA = 3-pyridineacrylic acid). **1** shows an interesting 1D ladder-like structure. As a bifunctional catalyst, **1** can be employed as a colorimetric sensor toward phenol with the relatively low detection limit (LOD) of 0.36 μmol/L (S/N = 3) in the wide range (0.001–0.1 mmol/L). The title colorimetric sensor is applied to determine phenol in various water environment with good recoveries ranging from 95%–105%. In addition, **1** also exhibits excellent photocatalytic degradation toward phenol under visible light with the highest removal efficiency at 96% for 100 min and wide pH universality. The selectivity, stability and reliability of the detection of **1** towards phenol, as well as the detection for 4-chlorophenol, *o*-cresol, 4-nitrophenol and phloroglucinol were studied. Furthermore, the photocatalytic reaction kinetics and the mechanisms of photodegradation of phenol were also investigated in detail.

Phenolic substances (phenol, 4-chlorophenol, 4-nitrophenol, *etc*) are widely used in food, medicine and industry, but many of these phenolic substances are discharged into the water as effluent, which has resulted in serious water pollution around the world [1–3]. We need an eco-friendly settlement that can detect and removal phenolic substances in wastewater [4–6]. Phenol is the most common pollutant of phenolic substances exist in wastewater and the World Health Organization (WHO) listed it as priority control pollutant in water due to its carcinogenic nature. As for the U.S. Environmental Protection Agency (EPA), the maximum permitted limit of phenol in drinking water is 1 μg/L [7–9]. To detect phenol in aqueous medium, some methods have been reported including chromatographic, spectrophotometric and electrochemical. Nevertheless, the colorimetric analysis is an effective method for detecting phenol owing to its high degree of precision, selectivity and sensitivity [10,11]. Besides that, the removal of phenol is extremely important, consequently, scientists are devoted to develop a new promising method with prominent efficiency. Many methods have been obtained for removing phenolic substances in wastewater such as biological treatment, adsorption extraction, chemical precipitation and membrane separation [12–14]. Compared with above methods, the photodegradation of phenolic substances is one of the promising method due to its low treatment cost and no secondary pollution [15,16]. Therefore, design and synthesis new catalysts for both trace detection and photodegradation of phenol is a challenging and meaningful work.

Polyoxometallates (POMs) with oxygen-rich surfaces and highly negative charges, have attracted more and more attention due to their interesting structural diversity and potential applications [17–26]. POM-based metal-organic complexes (POMOCs) as a branch of POMs, are often used as a catalytic material widely used in photo/electro-catalysis, electrocatalysis, adsorption, magnetism and other fields due to their excellent stability [27–32]. Researchers have reported several POMOCs to detect or removal phenolic substances. Ma *et al.* has obtained a new POMOC $[Co_2(btap)_4(H_2O)_4][SiW_{12}O_{40}]$ (btap = 3,5-bis(triazol-1-yl)pyridine) with two fold interpenetrated and displayed excellent colorimetric detection performance to phenol with LOD of 1.32 μmol/L [33]. Su *et al.* has synthesized a new POMOC hybridy $\{((Cu(bipy))_2(\mu\text{-}PhPO_3)_2Cu(bipy))_2H(PCuW_{11}O_{39})\cdot 3H_2O\}_n$ (bipy = 2,2′-bipyridine) used as biocatalyst for degradation of phenol, 4-chlorophenol

* Corresponding authors.
E-mail addresses: lgch1004@sina.com (G. Liu), zhangzhong666@126.com (Z. Zhang), wangxiuli@bhu.edu.cn (X. Wang).

https://doi.org/10.1016/j.cclet.2023.109148
1001-8417/

(4-CP) and 2,4-dichlorophenol (2,4-DCP) [34]. To our knowledge, the colorimetric analysis and photodegradation of phenol using a single material has not been well-explored. Hence, this study is highly significant and useful for industrial application.

In this work, we obtained a new POMOC by using Keggin-type $[SiW_{12}O_{40}]^{4-}$ (SiW_{12}) and 3-HPA ligand in presence of dap under solvothermal reaction, namely $\{[Cu(dap)(3\text{-}PA)]_4(SiW_{12}O_{40})(H_2O)_2\}\cdot 2H_2O$ (dap = 1,2-diaminopropane, 3-HPA = 3-pyridineacrylic acid) (**1**), and characterized it by elemental analysis, IR spectra, PXRD and UV–vis diffuse-reflectance. **1** as a peroxidase, evaluated through H_2O_2, and the oxidative coupling reaction of phenols and 4-aminoantipyrine (4-AAP) proves the good catalytic activity of **1**, a rapid colorimetric method for the determination of phenols was established. The LOD is only 0.36 μmol/L using **1** as a peroxidase mimic. Furthermore, **1** exhibits excellent photocatalytic degradation performance toward phenol with the removal efficiency of 96% for 100 min, and has satisfactory selectivity, stability and reliability.

Synthesis of $\{[Cu(dap)(3\text{-}PA)]_4(SiW_{12}O_{40})(H_2O)_2\}\cdot 2H_2O$ (**1**): A mixture of $Cu(NO_3)_2\cdot 3H_2O$ (0.50 g, 2.07 mmol), $H_4[SiW_{12}O_{40}]\cdot xH_2O$ (0.50 g, 0.17 mmol), 3-HPA (0.40 g, 2.68 mmol), 1,4-naphthalenedicarboxylic acid (1,4-H_2NDC) (0.20 g, 0.92 mmol), dap (0.2 mL), H_2O (4 mL) and acetonitrile (2 mL) was stirred for 2 h ($pH_{start} = 3.77$). The resulting mixture was added to a 25 mL Teflon-lined stainless steel reactor, then kept at 120 °C for 4 days and cooled to room temperature ($pH_{end} = 3.71$). Blue block crystals were filtered from solution, washed by ultrapure water and acetonitrile with a yield of 54% based on $H_4[SiW_{12}O_{40}]\cdot xH_2O$. Anal. calcd. for $C_{44}H_{70}Cu_4N_{12}O_{52}SiW_{12}$: C, 12.92; H, 1.73; N, 4.12. Found: C, 12.98; H, 1.81; N, 4.10. IR (KBr, cm^{-1}): 3558 (w), 3438 (w), 3324 (w), 3245 (w), 2954 (w), 2869 (w), 1641 (m), 1555 (s), 1464 (w), 1441 (s), 1362 (m), 1287 (w), 1259 (m), 1185 (w), 1071 (m), 1009 (m), 999 (m), 969 (m), 912 (m),873 (m), 775 (s), 696 (w), 633 (w), 537 (m). The crystallographic data structure refinement information and selected bond distances (Å) of **1** are summarized in Tables S1 and S2 (Supporting information), respectively.

Complex **1** used a mixture of $Cu(NO_3)_2\cdot 3H_2O$, $H_4(SiW_{12}O_{40})\cdot xH_2O$, 3-HPA, 1,4-$H_2$NDC, and H_2O at 120 °C for 4 days under solvothermal conditions. Although 1,4-H_2NDC was used as a starting material for the synthesis of **1**, 1,4-H_2NDC was not present in **1**. Exploratory experiments showed that **1** is not obtained under the same conditions after removal of 1,4-H_2NDC. The addition of 1,4-H_2NDC may provide a suitable solution environment for high-quality crystalline materials and play a role in mineralization [35]. During the synthesis of complex **1**, we carried out the parallel experiments under the same conditions. When replaced $Cu(NO_3)_2\cdot 3H_2O$ by $Cu(OAc)_2\cdot H_2O$ or $CuCl_2\cdot 2H_2O$, no blue crystal produced; when we added 0.1, 0.15, 0.2, 0.25 or 0.3 mL of dap respectively, the results showed that the same product was obtained in the range of 0.15–0.25; and we tried 100 °C, 120 °C, 140 °C, and only obtained crystals at 120 °C.

The results of Bond-valence-sum (BVS) calculations show that the valence of Cu, Si and W atoms in **1** are +2, +4 and +6 (Table S3 in Supporting information), verifying the charge balance of **1** [36]. Single crystal X-ray diffraction indicated that complex **1** crystallizes in triclinic space group *P*-1. The structure unit of **1** is consists of one $[SiW_{12}O_{40}]^{4-}$ anion, two $\{[Cu(dap)(3\text{-}PA)]_2(H_2O)\}^{2+}$ metal-organic units, and two lattice water molecules (Fig. 1a). $[SiW_{12}O_{40}]^{4-}$ anion presents a classic Keggin-type structure, and eight oxygen atoms surround the central atom Si in a semi-occupied manner [Si–O: 1.57(3)–1.71(3) Å, W–O: 1.66(3)–2.50(3) Å]. The 3-PA ligands exhibit *cis* and *trans* coordination modes: 3-PA-a and 3-PA-b. Two crystallographically independent Cu^{2+} ions (Cu1, Cu2) in **1**, which adopt pentacoordinated environment in a distorted square-pyramid geometry. Cu1 is coordinated with two N atoms from one dap ligand, one N atom from 3-PA ligand and one O atom from $\{SiW_{12}\}$ anion, while Cu2 bonds to two N atoms

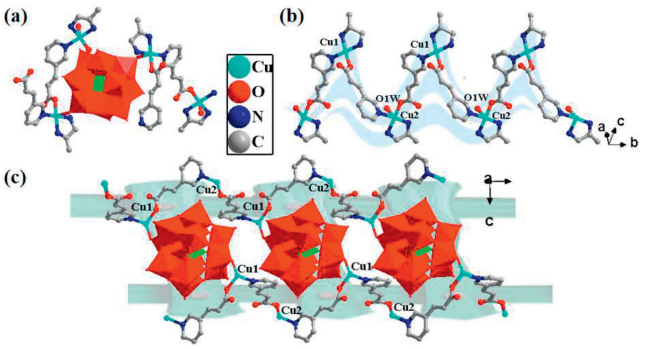

Fig. 1. (a) The structure unit of complex **1**. (b) Wave-like $\{[Cu(dap)(3\text{-}PA)]_2(H_2O)\}_n^{2n+}$ chain. (c) Nano-ladder (dap and coordinated water molecules are omitted for clarity).

from one dap ligand, one N atom from 3-PA ligand and one O atom from coordinated water molecule (Figs. S1a and b in Supporting information). Thus, the crystallographically independent Cu1 and Cu2 ions are linked by 3-PA-a and 3-PA-b in an alternate manner to form a wave-like 1D metal-organic chain along the *b*-axis (Fig. 1b, Figs. S1c and d in Supporting information). One dap and a coordinated water molecule decorate on both sides of the chain by coordinating with each Cu ion. Two mutually parallel $\{[Cu(dap)(3\text{-}PA)]_2(H_2O)\}_n^{2n+}$ chains are bridged by SiW_{12} anions and coordinated with Cu1 ions to generate a inorganic-organic nano-ladder (Fig. 1c and Fig. S1e in Supporting information). The Cu–O distances are in the range of 1.92(2)–2.15(2) Å and the Cu–N distances are from 1.97(2) to 2.06(2) Å] (Table S2). The adjacent chains were connected through H-bonds between carboxyllate oxygen and coordination water to form 2D supermolecular layer (Table S4 and Fig. S2 in Supporting information).

Up to now, only a few POMOCs constructed with 3-HPA have been reported, such as $(3\text{-}H_2PA)[(3\text{-}HPA)_2Ag][AgAlMo_6H_6O_{24}]\cdot 3H_2O$ (**2**), $[(3\text{-}HPA)_2Ag][(H_2O)_2Ag]_2[AlMo_6H_6O_{24}]\cdot 2H_2O$ (**3**) and $HNa_2[(3\text{-}PA)(3\text{-}HPA)Ag]_2[AlMo_6H_6O_{24}]\cdot 8H_2O$ (**4**) [37]. As we know, 3-HPA have shown free ligand (in **2**), monodentate ligand (in **3**) and *cis*-bidentate ligand (in **4**), respectively. It is interesting that 3-PA exhibits *cis* and *trans* bidentate coordination modes simultaneously in complex **1**.

Firstly, powder X-ray diffraction (PXRD) and IR spectroscopy were used to characterize the complex **1**. The detail information can be found in the supporting information. The simulated and experimental diffraction peaks are matches well, indicating that the phase purity of **1** is well (Fig. S3 in Supporting information). The FT-IR spectrum shows the bands at 999 cm^{-1}, 969 cm^{-1}, 948 cm^{-1} and 873 cm^{-1} are attributed to $\nu_{as}(W{=}O_d)$, $\nu_{as}(Si{-}O_a)$, $\nu_{as}(W{-}O_b{-}W)$, and $\nu_{as}(W{-}O_c{-}W)$, respectively. The absorption bands at 2869–2954 cm^{-1} and 1441–1555 cm^{-1} are corresponded to $-NH_2$ and $-CH_2$ group (Fig. S4 in Supporting information) [38]. Above results showed that the complex **1** were synthesized from the corresponding starting materials.

As we know that excessive amounts of phenolic compounds are harmful to biological tissue. Therefore, the detection of phenolic contaminants is very important [39,40]. Colorimetry can use color change to qualitatively or quantitatively detect substances. The determination process is simple and rapid, which attracts people's attention [41,42]. In order to explore the peroxidase-like characteristics of **1** (Fig. 2a), H_2O_2 was used as oxidant for the oxidative coupling reaction between phenol and 4-AAP. In the control experiment, only phenol and 4-AAP were added. In this system, when H_2O_2 and **1** are added, the solution changes from colorless to obvious pink by naked eyes, and the UV–vis peak at 503 nm is enhanced, which indicates that oxidative coupling reaction occurs.

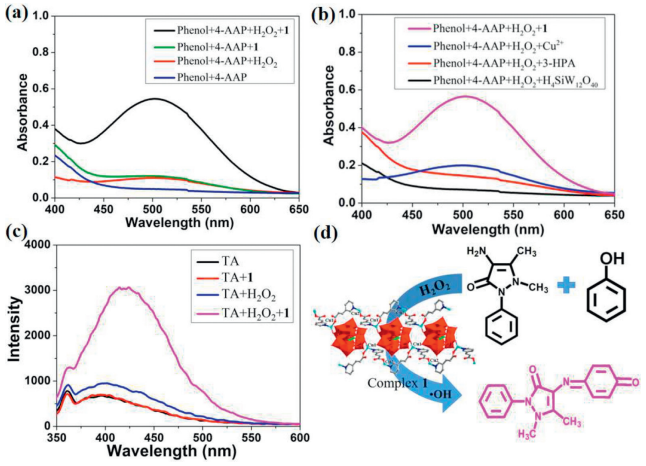

Fig. 2. (a, b) UV–vis absorbance spectra of diverse systems and various compounds (**1**, SiW_{12}, 3-HPA, Cu^{2+} at the same μmol). (c) ·OH-trapping photoluminescence spectra (0.5 mmol/L of TA, 0.5 mg/mL of **1**, 5 mmol/L of H_2O_2). (d) Proposed mechanism of phenol catalyzed by **1**.

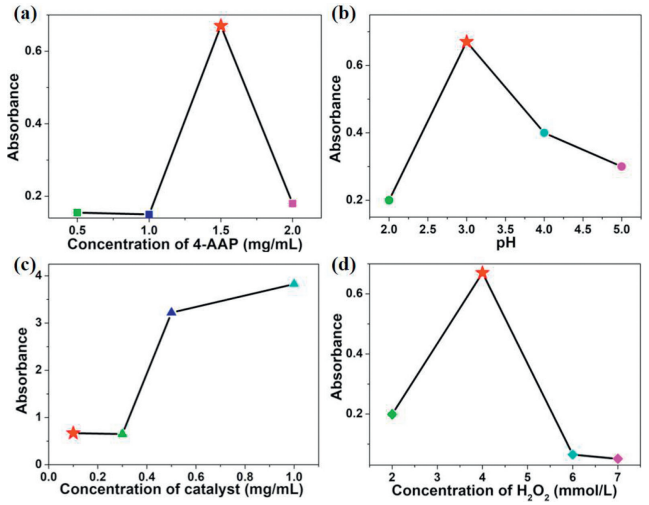

Fig. 3. Effect of (a) concentration of 4-AAP, (b) pH, (c) concentration of catalyst, (d) concentration of H_2O_2 on the colorimetric quantification of phenol.

When only H_2O_2, **1**, SiW_{12}, 3-HPA, or Cu^{2+} were added into the system, no obvious pink color was observed by naked eyes, and the UV–vis peak at 503 nm did not increase obviously, indicating that oxidative coupling reaction did not occur. The above phenomena indicated that **1** as a peroxidase mimic, could catalyze the H_2O_2 reaction of phenol and 4-AAP to form quinoneimine. In addition, the same molar mass of **1**, SiW_{12}, 3-HPA and Cu^{2+} were used in the system of phenol, 4-AAP and H_2O_2, the UV absorption peak was measured at 503 nm. The absorbance follows the order of **1** > Cu^{2+} > 3-HPA > SiW_{12} (Fig. 2b). The experimental results show that the activity of **1** as peroxidase mainly comes from the coordination of Cu^{2+} and 3-HPA, and the increase of absorbance may be due to the synergistic effect of metal and 3-HPA.

In previous reports, hydroxyl radicals (·OH) were usually involved in the reaction catalyzed by peroxidase mimetic. Therefore, photoluminescence experiments were used to explore the mechanism of **1** as a peroxidase mimetic [33]. Since peroxidase generate ·OH when carry out a catalytic reaction. Terephthalic acid (TA) was selected as a fluorescence probe to identify hydroxyl group, and carried out as follows: (I) TA; (II) TA and **1**; (III) TA and H_2O_2; (IV) TA, H_2O_2 and **1** in a 5 mL centrifuge tube and set the total volume to 3 mL, react in the dark for 12 h and centrifuge. Then, the fluorescence spectrum of the mixed solution was detected at an excitation wavelength of 326 nm. As shown in Fig. 2c, the fluorescence test results show that III and IV both have an absorption peak at 420 nm, and IV is higher than III solution. The results indicated that the peroxidase-like activity of **1** was mainly derived from ·OH generated by the decomposition of H_2O_2. ·OH can take electrons from the hydroxyl of phenols to produce quinone free radicals due to the outstanding oxidation capacity. Subsequently, the pink quinoneimine can be formed by the oxidative coupling of 4-AAP and quinone radicals (Fig. 2d) [43,44].

To make better use of the peroxidase activity of **1**, a colorimetric sensor for the quantitative analysis of phenolic pollutants (phenol/4-chlorophenol/*o*-cresol/4-nitrophenol/phloroglucinol) was designed. In order to make the best use of the phenol sensor system, the experimental conditions were optimized in a certain range. Similar to other reported enzyme mimics, the catalytic efficiency of **1** also depends on the amount of 4-AAP, pH, catalyst and H_2O_2. The best experimental conditions were explored by using phenol as a model. When the amount of 4-AAP is in the range of 0.5–2 mg/mL, the absorbance is the strongest at 1.5 mg/mL (Fig. 3a). Complex **1** exhibited peroxidase-like activity at acidic pH

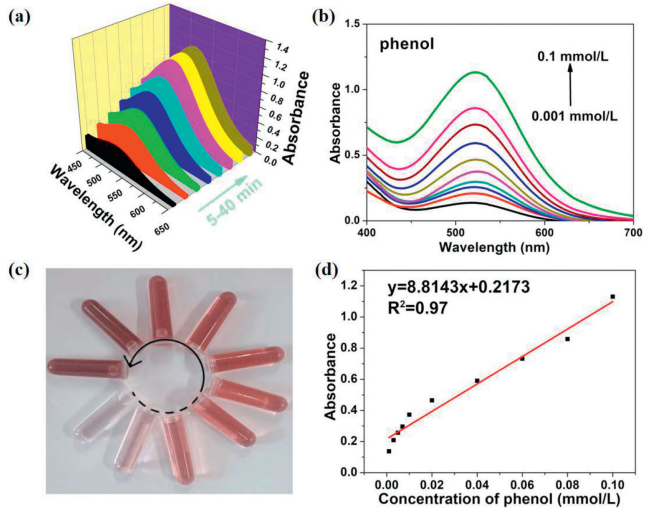

Fig. 4. (a) The absorbance (503 nm) changes of the phenol and 4-AAP system *vs.* time. (b) UV–vis absorbance spectra of the colorimetric detection of phenol in the **1** + H_2O_2 + 4-AAP system. (c) Photographs of different concentration of phenol added to the **1** + H_2O_2 + 4-AAP system. (d) The linear calibration curve for detection at varied phenol concentrations.

conditions and maximum activity was achieved at pH 3 (Fig. 3b). Meanwhile, the absorbance increases with the amount of catalyst **1** in the range of 0.1–1.0 mg/mL (Fig. 3c). Under the selected assay conditions, the absorbance is the strongest when the amount of H_2O_2 is 4 mmol/L (Fig. 3d). Therefore, the optimum conditions for determination are as follows: the concentration of 4-AAP is 1.5 mg/mL, the pH value is 3, the concentration of catalyst is 0.1 mg/mL, and the concentration of H_2O_2 is 4 mmol/L.

Under the optimal conditions, the absorbance was tested every 5 min, and the absorbance had no obvious change after 30 min (Fig. 4a). Then, phenol of different concentrations was added to 3 mL of solution containing **1** and 4-AAP, H_2O_2 (Fig. 4b). With the increase of phenol concentration, the color of the solution gradually changed from colorless to a distinct pink (Fig. 4c). The absorbance and the phenol concentration show a linear relationship over the range of 0.001–0.1 mmol/L (Fig. 4d). The limit of detection (LOD) for phenol (S/N = 3) was 0.36 μmol/L. As shown in Table 1, the LOD of composite materials are in the range of 0.86–3.33 μmol/L [9,15,16,45]. The corresponding value of POM-

Table 1
Comparative table for the detection of phenol using different enzyme mimics.

Catalysts	Linear range (μmol/L)	LOD (μmol/L)	Ref.
HRP@H-ZIF-8-GOx	0–100	0.86	[45]
Fe_3O_4 NPs	1.67–1200	3.79	[16]
Fe_3O_4/rGO/MOF	10–80	3.33	[9]
Co-MOF-74	0.5–300	1.02	[15]
Co-POM	10–1000	1.32	[29]
1	1–100	0.36	This work

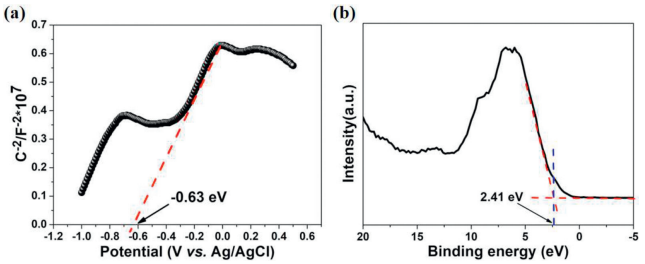

Fig. 5. (a) Mott-Schottky plot of **1**. (b) The VB-XPS of **1**.

based complex is 1.32 μmol/L [33]. The LOD of **1** is apparently lower than most of the enzyme mimetics that have been reported as colorimetric detectors for phenol. The detection limits for 4-chlorophenol, *o*-cresol, 4-nitrophenol and phloroglucinol were also satisfying (1.89, 2.12, 1.67 and 5.02 μmol/L) (Figs. S5a–h in Supporting information).

In order to verify the selectivity of phenol, the possible interference of coexisting species such as ethanol, acetone, NaCl and 2-ethylimidazole on phenolics was studied (Fig. S6a in Supporting information). Add above substances to the **1** + H_2O_2 + 4-AAP system, the color of the solution still colorless (Fig. S6b in Supporting information). The influence of the above reactions on phenol is almost negligible, which shows that they have good anti-interference performance in phenol analysis.

The method has been applied to the analysis of tap water (Jinzhou), industrial discharge water (a petrochemical plant) and lake water (Jinzhou, Bohai University). As shown in Table 2, the range of the recoveries toward above three samples is 95%–105%, and the corresponding RSDs were from 1.00% to 5.87% ($n = 3$). The concentration of phenol is proportional to the absorption intensity with good linear relationship (Fig. S7 in Supporting information). The above results indicated that the method was simple, reliable and sensitive for the visual detection of phenol derivatives in water environment.

In order to understand the photocatalytic performances of complex **1** in detail, firstly, the photocatalytic activities of **1** were evaluated by measurement of UV–vis absorption spectrum (Fig. S8a in Supporting information), the band gap energy (E_g) of **1** is 3.21 eV, which displays that **1** can be considered as a semiconductor material (Fig. S8b in Supporting information) [46,47]. As is well known, the Mott-Schottky (MS) electrochemical test can be used to obtain the Fermi level (E_f). As shown in Fig. 5a, the Fermi level E_f is −0.63 eV *vs.* Ag/AgCl (−0.43 eV *vs.* NHE) and the MS curve features positive slope. The above results show that **1** is a typical n-type semiconductor. The gap between the E_f and VB potentials of **1** was measured by the VB-XPS method, which is 2.41 eV (2.17 eV *vs.* NHE) (Fig. 5b). Therefore, the VB of **1** is 1.74 eV (*vs.* NHE) and the corresponding CB is −1.47 eV (*vs.* NHE) combining the band gap value (3.21 eV).

Complex **1** was used as photocatalyst to degradate phenol under visible light, and the removal efficiency is affected by various reaction conditions, including the pH, molar ratio of H_2O_2/phenol, amount of catalyst and concentration of phenol. Firstly, the pH range of 1–14 was selected due to the wide pH range in wastewater. As shown in Fig. 6a, with the increase of pH, the removal efficiency of phenol by complex **1** reaches the maximum (96%) at pH 7.5 in 100 min, and then it begins to decrease as pH continues to increase. The detected pH range (1–14) is apparently wider than most reported materials (Table S5 in Supporting information) [9,15,34]. The removal rate of phenol in 30 min is 65.8%, which is apparently higher than that of reported POM-based complex (Table S6 in Supporting information) [34]. As shown in Fig. 6b, the most appropriate molar ratio of H_2O_2/phenol is 46:1 at pH 7.5. The amount of catalyst is one of the key factors affecting the phenol removal efficiency, as shown in Fig. 6c, with the amount of **1** increase from 2.5 mg to 20 mg, the phenol removal efficiency reached the maximum at 5 mg. In addition, **1** exhibits outstanding removal ability for phenol solutions at the concentration of 200 mg/L and 400 mg/L. When the concentration is higher than 400 mg/L, the removal ability for phenol presents a reduction trend (Fig. 6d). Based on these results, we established the optimal photocatalytic degradation conditions; phenol concentration (400 mg/L), pH (7.5), reaction time (100 min), H_2O_2/phenol molar ratio (46:1) and catalyst **1** amount (5 mg) are used for photocatalytic degradation of phenol with the removal efficiency at 96%.

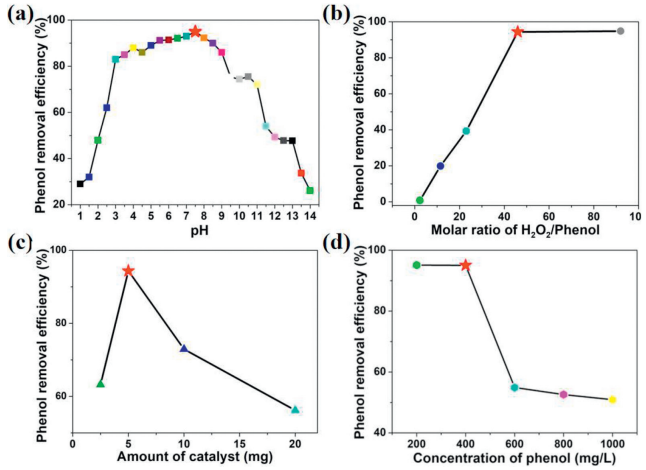

Fig. 6. The effects of (a) different pH, (b) molar ratio of H_2O_2/phenol, (c) amount of catalyst and (d) concentration of phenol on the phenol removal efficiency. Reaction conditions for (a): Reaction time (100 min), amount of **1** (5.0 mg), molar ratio of H_2O_2/phenol (46:1) and phenol concentration (400 mg/L); the conditions for (b-d) are the same as (a) except that the pH is 7.5.

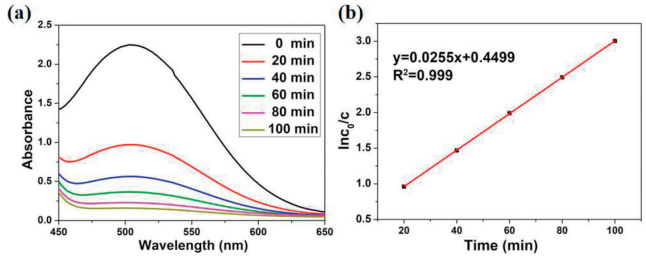

Fig. 7. (a) The photocatalytic degradation of phenol in presence of **1** under different irradiation times. (b) The linear relationship between $\ln(c_0/c)$ and reaction time (t) of phenol.

Fig. 7a shows the catalytic activity of complex **1** for phenol degradation under the optimal catalytic condition. The reaction kinetic of photocatalytic process is matched with the *pseudo*-first-order mode corresponding to Langmuir-Hinshelwood model [48,49], The color of the solution changed from pink to light yellow as the photocatalytic process proceeded (Fig. S9 in Supporting information). The $\ln(c_0/c)$ and reaction times of phenol shows an excellent linear relationship with R^2 of 0.999 [50,51]. The appearance rate constant and corresponding half-life of **1** for phenol is 0.0255

Table 2
Results for the determination of the phenol in three water samples.

Sample	Original amount (mmol/L)	Added (mmol/L)	Found (mmol/L)			Recovery (%)			RSD (%)
			1	2	3	1	2	3	
Tap water	N.D.[a]	0.002	0.0019	0.0021	0.0019	95.00	105.00	95.00	5.87
		0.006	0.0062	0.0058	0.0061	103.30	96.67	101.67	3.44
		0.01	0.0099	0.0101	0.0099	99.00	101.00	99.00	1.16
Industrial discharge water	N.D.[a]	0.002	0.0021	0.0019	0.0020	105.00	95.00	100.00	5.00
		0.006	0.0057	0.0061	0.0058	95.00	101.67	96.67	3.55
		0.01	0.0101	0.0099	0.0100	101.00	99.00	100.00	1.00
Lake water	N.D.[a]	0.002	0.0019	0.0021	0.0021	95.00	105.00	105.00	5.68
		0.006	0.0061	0.0057	0.0057	101.67	95.00	95.00	3.96
		0.01	0.0099	0.0101	0.0101	99.00	101.00	101.00	1.15

[a] N.D., not detected.

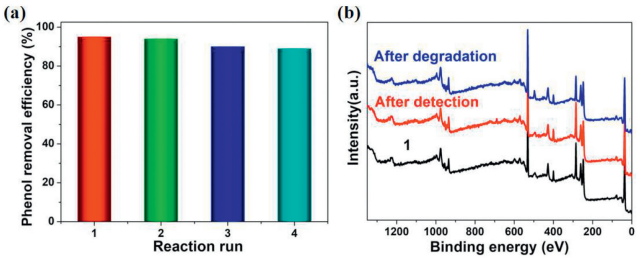

Fig. 8. (a) The removal efficiency of phenol after four cycles. (b) The XPS spectra patterns of **1** before and after detection/photoreduction of phenol.

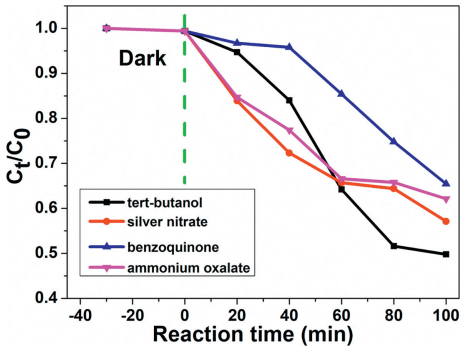

Fig. 9. The phenol removal efficiency in the presence of different sacrificial agents under visible light irradiation.

min^{-1} and 27.18 min (Fig. 7b), respectively. And we also study the catalytic activity of other starting material for phenol degradation under the optimal catalytic condition (Fig. S10 in Supporting information). We found that the phenol removal efficiency of 3-HPA, SiW_{12} and Cu^{2+} are only 38%, 43%, 46%. The above results prove that **1** is an efficient catalyst for the removal of phenol. Furthermore, the removal efficiency of phenol for complex **1** indicated no apparent changes after four recycling experiments (Fig. 8a). The XPS (Fig. 8b), PXRD (Fig. S11 in Supporting information) and IR (Fig. S12 in Supporting information) before and after detection and four times photocatalytic degradation reactions were not changed obviously, indicating that **1** has good structural stability.

In order to study the mechanism of photocatalytic degradation process, the reactive species trapping experiments were carried out [52,53]. SN (silver nitrate, 0.01 mol/L), AO (ammonium oxalate, 0.01 mol/L), TBA (*tert*–butanol, 0.01 mol/L), and BQ (benzoquinone, 0.01 mol/L) were introduce to scavenge e^-, h^+, ·OH, and $\cdot O_2^-$, the removal efficiency of phenol decrease to 43%, 38%, 51% and 35%, respectively (Fig. 9). The results show that the photocatalytic degradation process of phenol is affected by e^-, h^+, ·OH, $\cdot O_2^-$ together, while $\cdot O_2^-$ plays a major role.

As shown in Fig. 10, the mechanism of phenol photocatalytic degradation is explicated. The photogenerated electrons and

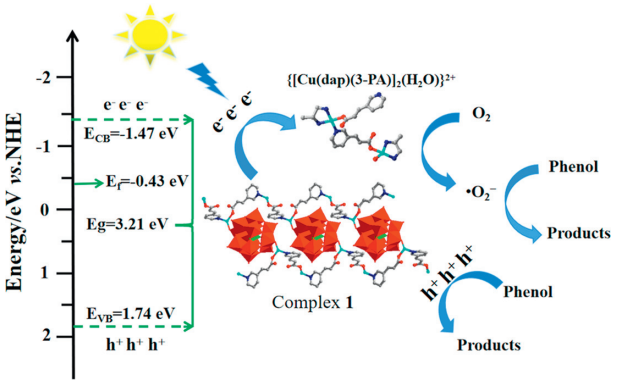

Fig. 10. Catalytic mechanism of **1** in the phenol degradation process.

holes on the surface of **1** are separated under light irradiation. The $\{[Cu(dap)(3\text{-}PA)]_2(H_2O)\}^{2+}$ metal-organic units connecting $[SiW_{12}O_{40}]^{4-}$, thus facilitate the electrons transfer between $[SiW_{12}O_{40}]^{4-}$ fragments through $\{[Cu(dap)(3\text{-}PA)]_2(H_2O)\}^{2+}$ units. This impetus can prevent from recombining electron-hole. Subsequently, the interplay between photogenerated electrons and oxygen molecules could to generate superoxide radicals, which can oxidize phenols to produce water and carbon dioxide. Meanwhile, the photogenerated holes and phenols directly response to the form products. The reduced $[SiW_{12}O_{40}]^{4-}$ can be rapidly re-oxygenated in the presence of O_2 to enter the next cycle [23,54,55].

In this paper, a new keggin-type POMOC was successfully synthesized and acted as a bifunctional catalyst to detect and degrade phenol. The results display that complex **1** is an excellent colorimetric detector with the detection limit (LOD) of 0.36, 1.89, 2.12, 1.67 and 5.02 μmol/L (S/N = 3) toward phenol, 4-chlorophenol, *o*-cresol, 4-nitrophenol and phloroglucinol, possessing satisfactory anti-interference. Moreover, complex **1** exhibits outstanding photocatalytic degradation activity toward phenol in the wide pH range with the highest removal efficiency at 96% for 100 min at pH 7.5, and the photocatalytic degradation process obeyed the pseudo-first-order reaction kinetic with the appearance rate constant and corresponding half-life of 0.0255 min^{-1} and 27.18 min, respectively. This work provides much stimulation to develop new POMOCs as bifunctional catalysts to detect and degrade phenolic substances in wastewater.

Declaration of competing interest

The authors declare no conflict of interest.

Acknowledgments

This work was supported by the National Natural Science Foundation of China (NSFC, Nos. 21901018, 21971024, 22271021), the Natural Science Foundation and Education Department of Liaoning province (Nos. 2022-MS-373, 2021-MS-312, LJ2020008).

Supplementary materials

Supplementary material associated with this article can be found, in the online version, at doi:10.1016/j.cclet.2023.109148.

References

[1] D.W. Li, Y. Cheng, H. Zuo, et al., J. Colloid. Interface. Sci. 603 (2021) 771–782.
[2] S. Ray, S. Panjikar, R. Anand, ACS Sens. 2 (2017) 411–418.
[3] Y. Gong, X. Zhao, H. Zhang, et al., Appl. Catal. B 233 (2018) 35–45.
[4] X.H. Zhong, Y. Lu, F. Luo, et al., Chem. Eur. J. 24 (2018) 3045–3051.
[5] W. Xu, Y.F. Zhang, X. Zhang, X.X. Xu, Q. Wang, J. Haz. Mat. 457 (2023) 131776.
[6] O.G. Sas, M. Castro, Á. Domínguez, B. González, Sep. Purif. Technol. 227 (2019) 115703.
[7] T. Dogan, E. Bayram, L. Uzun, S. Senel, A. Denizli, Inc. J. Appl. Polym. Sci. 132 (2015) 41981–41987.
[8] Q. Wang, X.Y. Wang, H. Wei, Anal. Chem. 94 (2022) 10198–10205.
[9] Y. Wang, M.Z. Zhao, C. Hou, et al., J. Taiwan. Inst. Chem. E 102 (2019) 312–320.
[10] N.N. Xing, Y.S. Lyu, J. Yang, et al., Environ. Sci. Nano 9 (2022) 2815–2826.
[11] S.Z. Huang, Q. Tang, K.N. Wei, et al., Anal. Chim. Acta 1233 (2022) 340504.
[12] T. Song, C. Xie, Q. Che, P. Yang, J. Ind. Eng. Chem. 122 (2023) 415–425.
[13] Y. Yuan, W.G. Pan, R.T. Guo, et al., Sep. Purif. Technol. 297 (2022) 121538.
[14] X. Chen, R.T. Guo, W.G. Pan, et al., Appl. Catal. B: Environ. 318 (2022) 121839.
[15] C. Hou, L.H. Fu, Y. Wang, et al., Carbohyd. Polym. 273 (2021) 118548.
[16] S.W. Wu, D.Z. Guo, X.C. Xua, J.M. Pan, X.H. Niu, Sensor. Actuat. B: Chem. 303 (2020) 127225.
[17] D. Zhang, W.Q. Zhang, Z.G. Lin, et al., Inorg. Chem. 59 (2020) 9756–9764.
[18] Z. Zhang, Y.L. Wang, Y. Liu, S.L. Huang, G.Y. Yang, Nanoscale 12 (2020) 18333–18341.
[19] L. Yang, Z. Zhang, C.N. Zhang, et al., Inorg. Chem. Front. 9 (2022) 4824–4833.
[20] X.T. Wang, W.J. Mao, D.S. Wang, et al., Talanta 257 (2023) 124270.
[21] B.X. Zeng, Y.Z. Li, G.P. Liu, et al., Inorg. Chem. 62 (2023) 10351–10358.
[22] R.D. Lai, Z.K. Zhu, Y.L. Wu, et al., Inorg. Chem. 61 (2022) 21047–21054.
[23] Y. Guan, H.P. Xiao, X.X. Li, S.T. Zheng, Polyoxometalates 2 (2023) 9140023.
[24] X.X. Li, C.H. Li, M.J. Hou, et al., Nat. Commun. 14 (2023) 5025.
[25] S.R. Li, W.D. Liu, L.S. Long, L.S. Zheng, X.J. Kong, Polyoxometalates 2 (2023) 9140022.
[26] X.X. Li, T. Ji, J.Y. Gao, et al., Chem. Sci. 13 (2022) 4573–4580.
[27] J.C. Liu, J.F. Wang, Q. Han, et al., Angew. Chem. Int. Ed. 60 (2021) 11153–11157.
[28] Q.Z. Wang, B.J. Xu, Y.Y. Wang, et al., Inorg. Chem. 60 (2021) 7753–7761.
[29] X.L. Wang, J.Y. Zhang, Z.H. Chang, et al., Inorg. Chem. 60 (2021) 3331–3337.
[30] D. Liu, B.K. Chen, J. Li, et al., Inorg. Chem. 60 (2021) 3909–3916.
[31] Y.N. Liu, J. Wang, L.N. Li, et al., Chem. Mater. 35 (2023) 3941–3950.
[32] S.Z. Chang, H.Y. An, Y.H. Chen, et al., ACS. Sustain. Chem. Eng. 10 (2022) 4728–4740.
[33] J.J. Xin, H.J. Pang, Z.X. Jin, et al., Inorg. Chem. 61 (2022) 16055–16063.
[34] Y. Lu, T. Zhang, Y.X. Zhang, et al., Dalton. Trans. 50 (2021) 15198–15209.
[35] Z.Y. Du, Z. Chen, R.K. Kang, et al., Inorg. Chem. 59 (2020) 12876–12883.
[36] I.D. Brown, D. Altermatt, Acta. Crystallogr. B 41 (1985) 244–247.
[37] Y. Hu, H.Y. An, X. Liu, et al., Dalton. Trans. 43 (2014) 2488–2498.
[38] R.J. Liu, X.K. Shang, C.X. Li, et al., Int. J. Hydrogen. Energ. 38 (2013) 9954–9960.
[39] Y.J. Jang, V.K.H. Bui, P.T. Nguyen, Y.C. Lee, M.I. Kim, Chemosensors 9 (2021) 219–228.
[40] T.S. Cheng, M.Z.M. Nasir, A. Appl. Mater. Today 9 (2017) 212–219.
[41] A. Saeed, M. Umer, N. Yamasaki, et al., ChemElectroChem 7 (2020) 3943–3950.
[42] S.R. Jia, X.K. Zhang, F. Yuan, T. Xia, ChemistrySelect 7 (2022) e202202984.
[43] D.P. Li, Y.L. Tong, J. Huang, et al., J. Mol. Catal. A: Chem. 345 (2011) 108–116.
[44] Y.H. Xiong, S.H. Chen, F.G. Ye, et al., Anal. Methods 7 (2015) 1300–1306.
[45] H.J. Liu, Y.J. Du, J. Gao, et al., Ind. Eng. Chem. Res. 59 (2020) 42–51.
[46] Z.W. Guo, L.H. Lin, J.P. Ye, et al., Angew. Chem. Int. Ed. 62 (2023) e202305260.
[47] R.G. Yang, Y.M. Fu, X. Meng, et al., Inorg. Chem. Front. 10 (2023) 3699.
[48] F.L. Wang, Y.P. Feng, P. Chen, et al., Appl. Catal. B 227 (2018) 114–122.
[49] M.F. Atitar, A. Bouziani, R. Dillert, M. Azzouzib, D.W. Bahnemann, Catal. Sci. Technol. 8 (2018) 985–995.
[50] R. Farouq, J. Chin. Chem. Soc. 65 (2018) 1333–1339.
[51] Z.H. Wang, C.Z. Wang, C.W. Zhang, W.J. Li, Innov. Food. Sci. Emerg. 44 (2017) 224–234.
[52] T.T. Cao, T.F. Xu, F.X. Deng, W.W. Qiao, C.W. Cui, J. Photoch. Photobio. A 407 (2021) 113025.
[53] E.F. Grosu, C. Gabriela, R. Froidevaux, Res. Chem. Intermediat. 44 (2018) 7731–7752.
[54] L.H. Yuan, J. Chai, S.W. Wang, et al., Environ. Technol. Innov. 30 (2023) 103085.
[55] K.F. Zhang, Y.X. Liu, J.G. Deng, et al., Appl. Catal. B: Environ. 224 (2018) 350–359.